SUPPLEMENTARY FOR

Quantifying daily NO_x and CO_2 emissions from Wuhan using satellite observations from TROPOMI and OCO-2

Qianqian Zhang[1,2], K. Folkert Boersma[1,3], Bin Zhao[4], Henk Eskes[3], Cuihong Chen[5], Haotian Zheng[4], Xingying Zhang[2]

[1] Wageningen University, Environmental Science Group, Wageningen, the Netherlands

[2] Key Laboratory of Radiometric Calibration and Validation for Environmental Satellites, Innovation Center for Fengyun Meteorological Satellite (FYSIC), National Satellite Meteorological Center, China Meteorology Administration, Beijing, 100081, China

[3] Royal Netherlands Meteorological Institute, De Bilt, the Netherlands

[4] State Key Joint Laboratory of Environmental Simulation and Pollution Control, School of environment, Tsinghua University, Beijing 100084, China

[5] Satellite Application Center for Ecology and Environment, Ministry of Ecology and Environment of the People's Republic of China, Beijing, 100094, China

Correspondence to: K. Folkert Boersma, folkert.boersma@wur.nl, Qianqian Zhang, zhangqq@cma.gov.cn

1. Emission spatial patterns

In the process of fitting the NO_x emissions from Wuhan, we give a first guess of spatial pattern of NO_x emission, i.e. the spatial pattern from the MEIC-2017 and ABACAS-2017 bottom-up inventories (blue and black lines in Fig. S1). To be mentioned, for each particular day, we let it shift along the wind direction, and finally obtain the fitted NO_x emission spatial pattern (red line in Fig. S1).

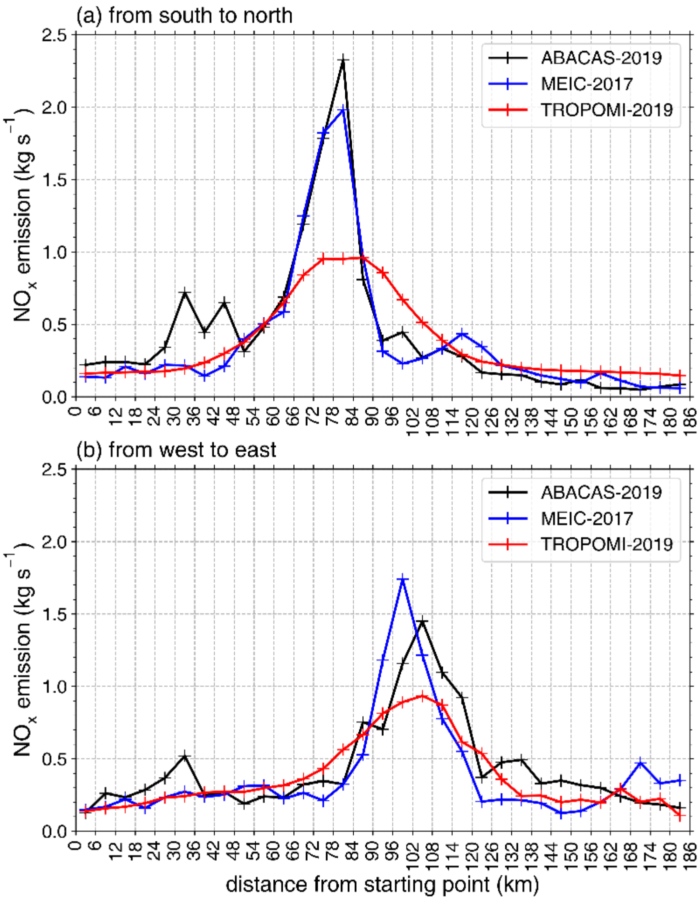

Figure S1: Spatial pattern of NO_x emissions in Wuhan from ABACAS-EI, MEIC and our fitted results.

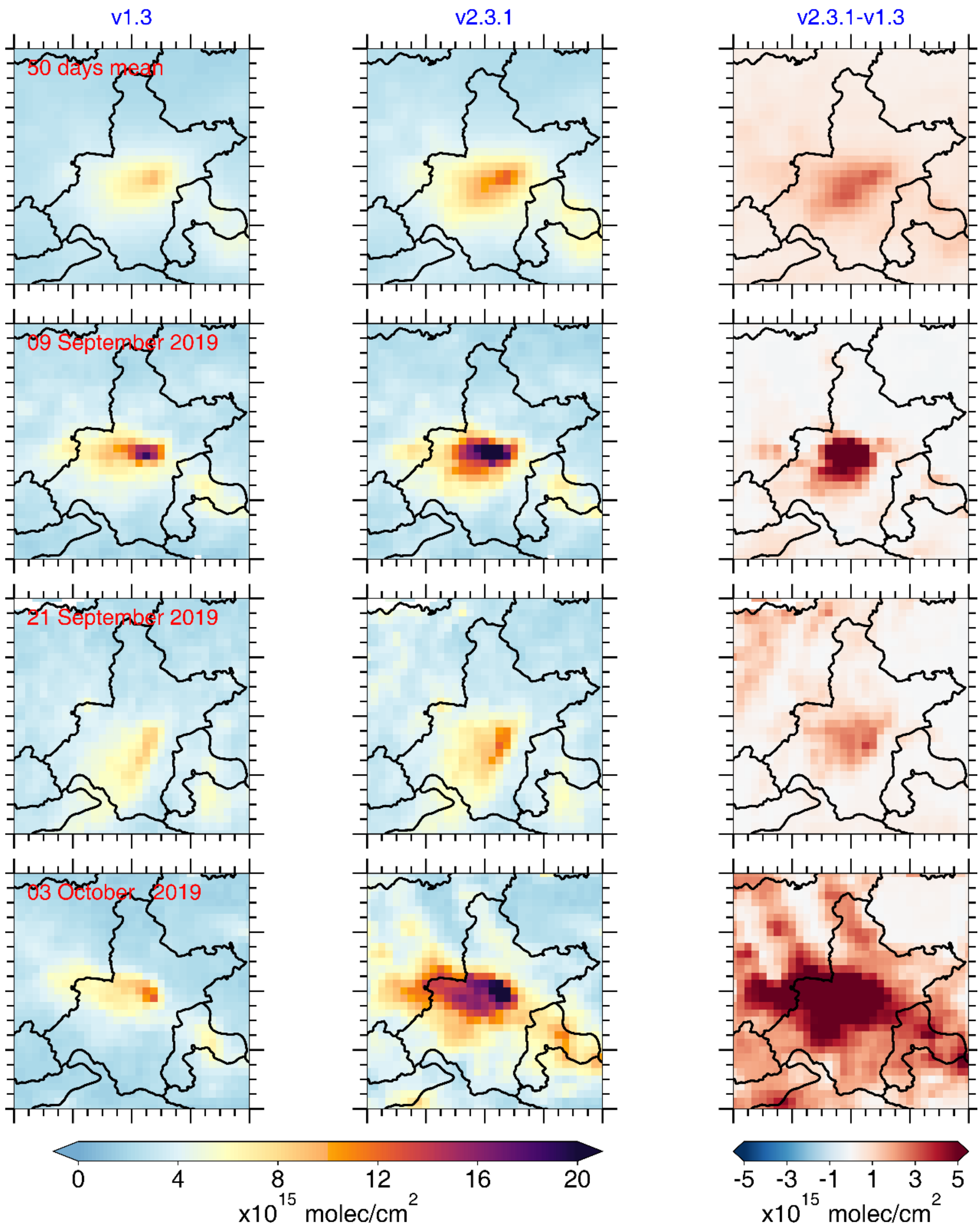

Figure S2: the difference in tropospheric NO_2 column densities between the version 2.3.1 and version 1.3 of TROPOMI data. From top to bottom: the 50 valid days mean in the study period, 09, 21 September and 03 October 2019.

2. Data input into the model besides satellite data and bottom-up emissions

We use the 12.1 version of GEOS-Chem model, with a horizontal resolution 0.25° × 0.3125° (~ 30 × 37.5 km^2) to provide the a priori guesses for chemical parameters relevant to daytime NO_x. The satellite overpasses at around 13:30 local time, when NO_2 is mainly subject to first-order loss with reaction to the hydroxyl radical (OH). The loss rate for NO_x is expressed as $k = \frac{k' \times [OH]}{[NO_x]/[NO_2]}$, where k' is the first-order reaction rate constant (2.8×10^{-11} cm^3/molec/s according to the GEOS-Chem model), $[NO_x]/[NO_2]$ is the mean ratio between NO_x and NO_2 within the boundary layer. We calculated from GEOS-Chem the boundary layer mean NO_x/NO_2 ratio over Wuhan to be 1.26 from September 2019 to August 2020 over Wuhan, and use the annual mean value 1.26 in the fitting, and it is close to that used in Liu et al. (2016) (1.32).

The OH concentration is highly uncertain and in-situ observations are sparse. In this study, we use GEOS-Chem model simulated boundary layer mean OH concentration at 13:00 local time as our first guess and allow it to change by ±20% in the fitting procedure. In addition, OH simulations from the CMAQ model that has a higher spatial resolution are used as a reference. The fraction of boundary layer NO_2 columns of the tropospheric total is also from GEOS-Chem and places typically about 90% of tropospheric NO_2 columns within the boundary layer.

Boundary layer mean wind fields are from ERA5, the fifth generation ECMWF atmospheric reanalysis of the global climate (Hersbach et al., 2020). We use the 05:00 UTC time (13:00 Wuhan time) zonal and meridional winds, with a horizontal resolution of 0.25° × 0.25°. Mean wind speed within boundary layer is calculated using the average of the wind speeds at all vertical layers within the boundary layer weighted by the NO_2 columns within each vertical layer. Considering that the wind field has a strong influence on the distribution of NO_2 column patterns, and thus on the NO_x emission estimation, we filter the TROPOMI NO_2 data based on the wind fields. After excluding the days with fluctuating wind direction (if wind direction changes more than 45 degrees in the hours before TROPOMI overpass) within the study domain, we finally obtain 50 days out of the ensemble of 81 valid satellite days between 1 September 2019 to 31 August 2020 to estimate NO_x and CO_2 emissions from Wuhan. The fraction of useful days is comparable to what Lorente et al. (2019) obtained for Paris, which is 27 days in 5 months.

3. NO_2 line density

This part demonstrates the way to achieve the 1-D distribution of satellite observed NO_2 along wind direction. First we define the study domain, the red circle in Fig. S3, including the whole area of Wuhan, as well as other small cities around Wuhan (The blue circle is the Third Ring Road of Wuhan, ~50% of NO_x emissions in the red circle are within the blue circle). First, we resample the TROPOMI NO_2 data at 6km×6km spatial resolution and rotating toward the wind direction, for our study domain, we get 31×31 grid cells. Second, we divide the 31×31 grid cells into 31 'line cells' along the wind direction, as shown with the pink grids in Fig. S3. Each cell is 186km wide (perpendicular to wind direction) and 6km long (along wind direction). Third, the NO2 line density (molec/cm) within each line cell is calculated through accumulating NO_2 column density (molec/cm^2) of all the 31 grid cells within the line cell, then we obtain the NO2 line density along wind direction as shown in the right panel of Fig. S3.

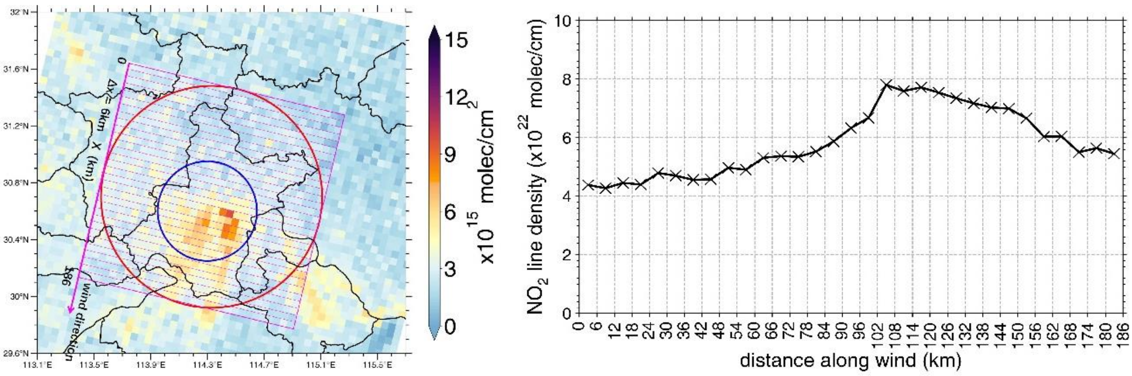

Figure S3. Left panel: tropospheric NO_2 column on May 18th 2020. The data is sampled with 0.05° (lon) × 0.05° (lat) grid size (~6×6km^2) and rotated toward the wind direction. The red circle centered at 114.3°E, 30.7°N represents our study domain, with a diameter of ~186km (31 cells along wind and 31 cells perpendicular to wind), and the blue circle defines the area within the Third Ring Road of Wuhan. For each cell along wind, 31 cells perpendicular to wind are accumulated to make up the line density of NO_2 (right panel).

4. Robustness with respect to the area of study domain

We choose a relatively large area as our study domain (a circular region centered at 114°E, 30.7°N, with a diameter of ~186km, Fig. S3 left panel, red circle.) to ensure the whole area of Wuhan are included. However, according to the bottom-up emission inventories (Fig. S1), more than 50% of the NO_x emissions in this area are concentrated within the Third Ring Road of Wuhan (84 km diameter, Fig. S3a the blue circle). The large study domain (186km wide of each cell along the NO_2 line density) may smear off the build-up of NO_2 in the high-emission area, and thus impact the estimated NO_x lifetime and emissions. To verify the robustness of our model to the area of the study domain, we randomly choose 3 days (08 September 2019, 10 November 2019, and 07 March 2020), narrow down the study domain to the blue circle in Fig. S3. In Fig. S4 we compare NO_x lifetimes and emissions from the inside of the Third Ring Road of Wuhan between the two situations with different area size of study domain.

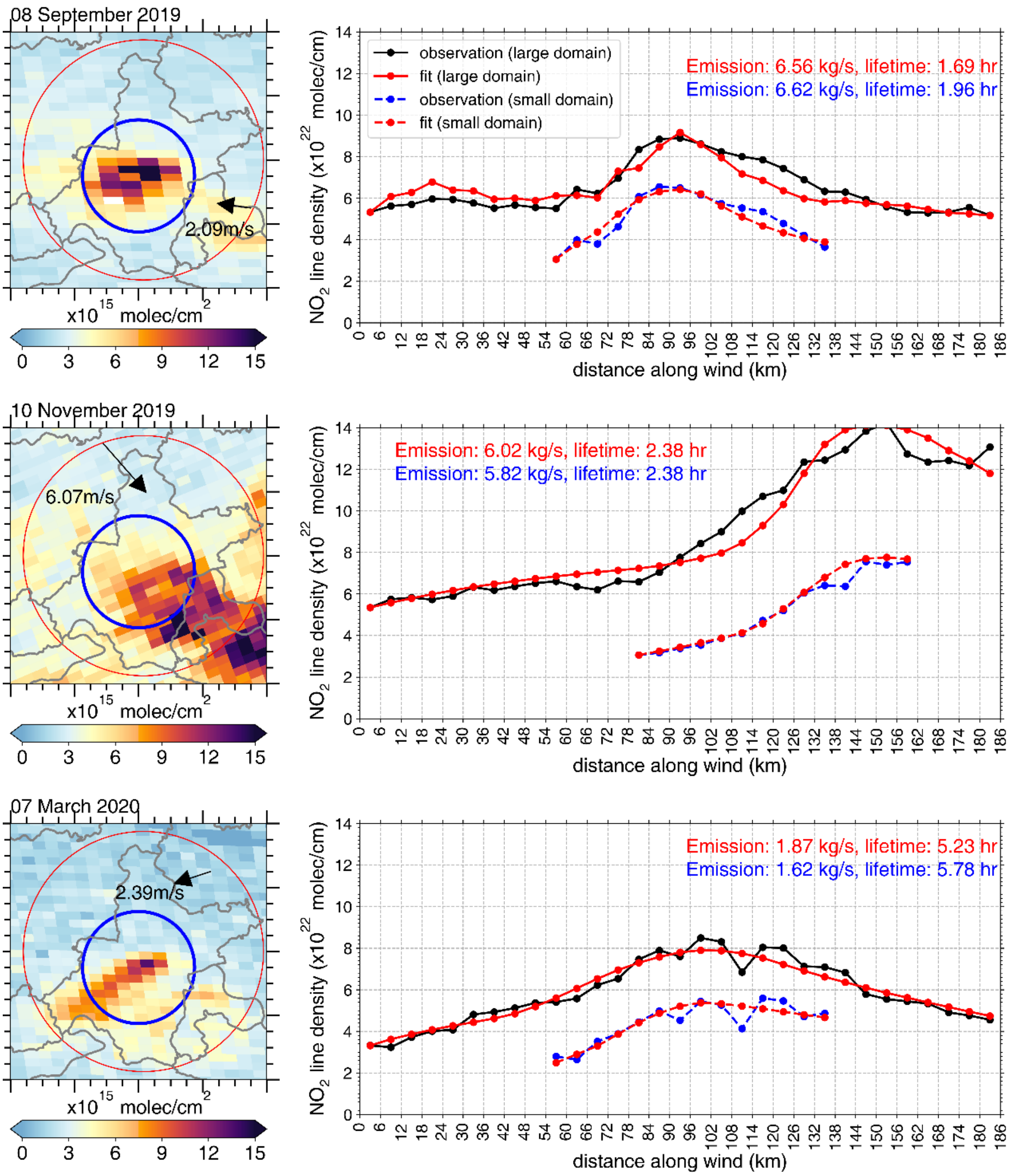

Figure S4. A comparison of NO_x emissions and lifetimes inside the Third Ring Road of Wuhan (blue circles in the left panel) using the superposition model under the two situations with large (red circles in left panel) and small (blue circles in left panel) study domains. NO_x emissions and lifetimes within the Third Ring Road of Wuhan are listed in right panel.

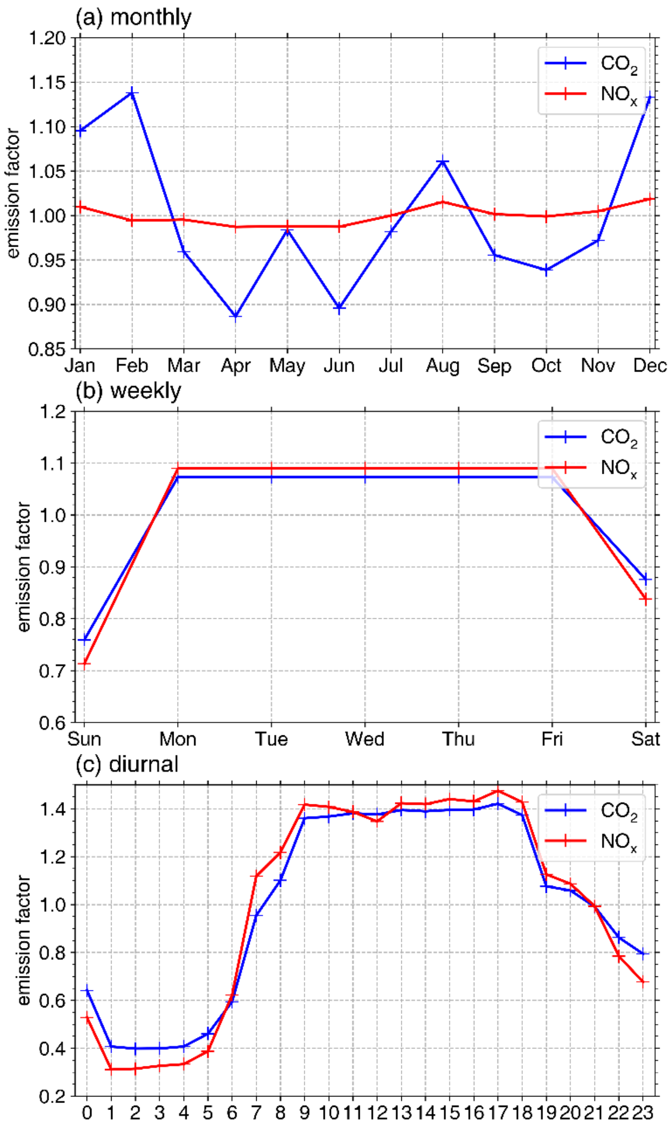

Figure S5. The (a) monthly, (b) weekly and (c) diurnal variation of NO_x and CO_2 emissions from Wuhan. The time factor is provided by ABACAS-EI, MEIC and GEOS-Chem model.

5. The Gaussian plume model.

To compare with the results from our superposition column model, we further use a Gaussian plume model (Bovensmann et al., 2010; Zheng et al., 2020) to estimate the XCO_2 enhancement due to Wuhan CO_2 emissions. XCO_2 enhancement on each point of the satellite orbit is contributed from the sum of all CO_2 emissions on the upwind region of the orbit:

$$C_{CO_2} = \sum \frac{E_{CO_2}}{\sqrt{2\pi} \times a \times u \times x^{0.894}} \times EXP[-\frac{1}{2}\left(\frac{y}{a \times x^{0.894}}\right)^2] \quad (1)$$

$$XCO_2 = C_{CO_2} \times \frac{M_{air}}{M_{CO_2}} \times \frac{g}{P_{surf} - w \times g} \times 10^3 \quad (2)$$

In Eq. (1), E_{CO_2} denotes the top-down CO_2 emission (g/s) and C_{CO_2} is the CO_2 column concentration enhancement (g/m^2) relative to the background. u is wind speed in m/s, $x\ (km)$ and $y\ (m)$ are the along wind and across wind distance from the location of the point emission source, respectively. a is the atmospheric stability parameter and the value is taken following Masters and Ela (2007). Eq. (2) is performed to convert C_{CO_2} to XCO_2, in which M_{air} and M_{CO_2} are the molecular weight of air and CO_2, g is the gravitational acceleration 9.8m/s^2. P_{surf} is the surface pressure (Pa) and w is the total column water content (kg/m^2), both of which can be accessed from the second Orbiting Carbon Observatory (OCO-2) satellite data file.

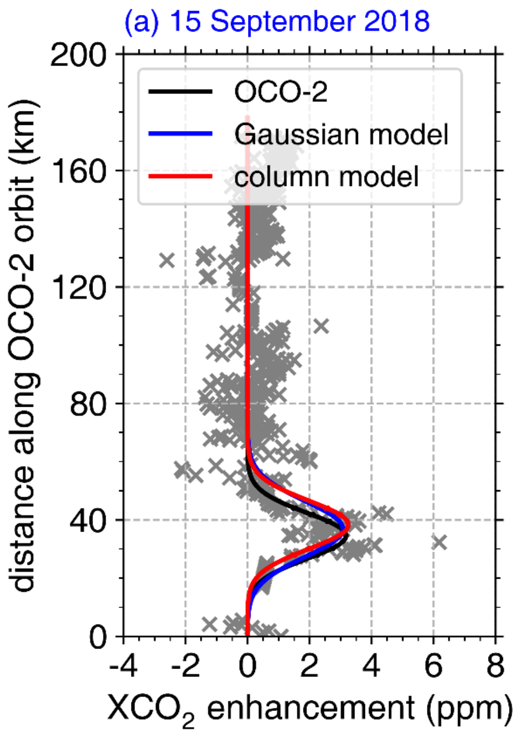

Figure S6. XCO_2 enhancement observations from OCO-2 (gray dots and black lines), and estimation with our top-down CO_2 emissions from the Gaussian plume model (blue lines) and the superposition model (red lines) on (a) 15 September 2018 and (b) 13 April 2020.

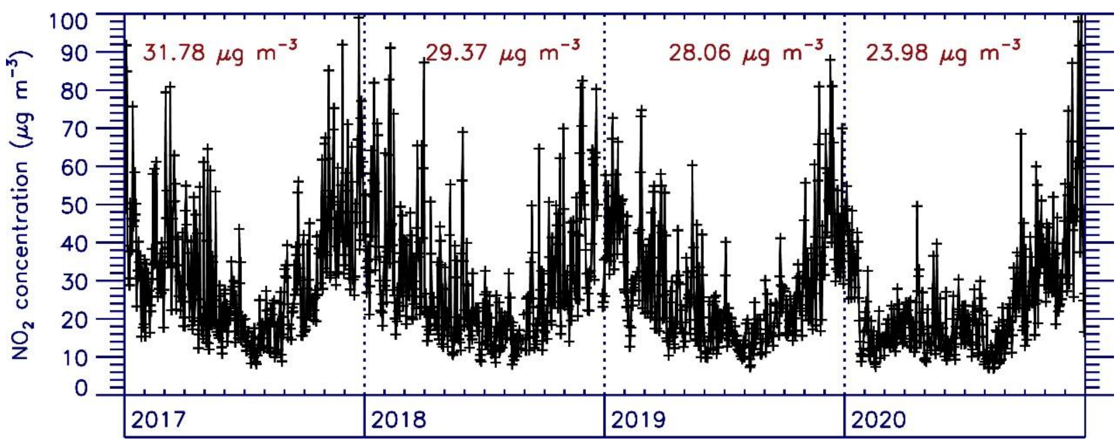

Figure S7. Daily noontime (13:00 and 14:00 mean) surface observed NO_2 concentration from 2017 to 2020. The annual mean concentration for each year is listed. The data is from the China National Environmental Monitoring Center (CNEMC) network, including 11 sites in Wuhan.

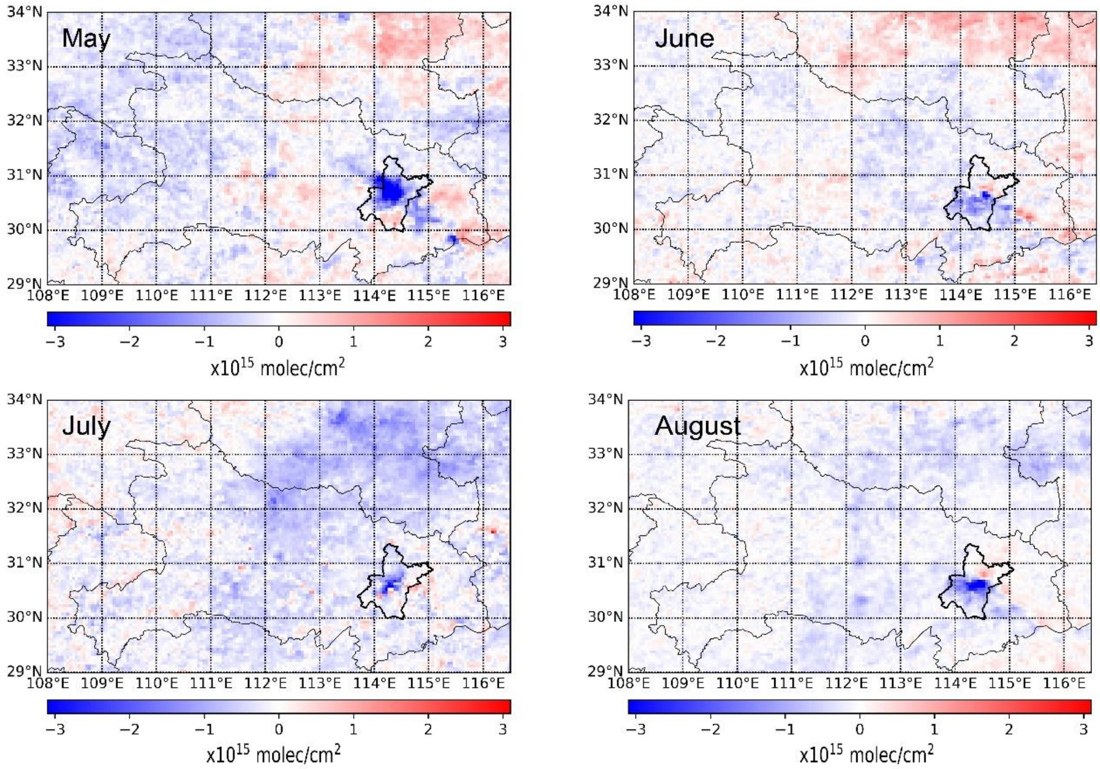

Figure S8. Difference in monthly mean NO_2 column between 2020 and 2019 (2020 minus 2019) over Hubei Province.

Table S1. NO_x and CO_2 emissions over Wuhan inferred from TROPOMI and related information of 50 days from September 2019 to August 2020.

day		NO_x emission (kg/s)	NO_x lifetime (hrs)	CO_2-to-NO_x Emission ratio (g CO_2/g NO_x)	CO_2 emission (kt/s)	wind speed (m/s)	wind direction (°)	back_offset × 10^{22} molec/cm	back_slope (× 10^{-22} molec/cm^2)	surface temperature (℃)	PBL height (m)	initial GC OH concentraion (molec/cm3)	initial CMAQ OH concentration (molec/cm^3)	OH concentration best fit (molec/cm^3)	R
2019/9/8	Tue	11.51±0.59	1.71±0.10	533	6.13±0.31	2.1	59 (ENE)	4.89E+22	-0.002	35	1274	7.63E+06	1.51E+07	7.31E+06	0.91
2019/9/9	Wed	10.60±1.02	1.29±0.03	533	5.65±0.54	2.64	111 (ESE)	4.42E+22	0.001	35	1321	8.17E+06	1.50E+07	9.69E+06	0.96
2019/9/21	Mon	12.65±0.93	1.89±0.07	533	6.74±0.5	10.6	22 (NNE)	4.73E+22	-0.004	27	1652	7.29E+06	1.37E+07	6.61E+06	0.92
2019/9/22	Tue	12.58±1.07	1.44±0.03	533	6.7±0.57	9.92	29 (NNE)	6.11E+22	-0.01	28	1569	7.97E+06	1.24E+07	8.68E+06	0.95

2019/9/23	Wed	12.18±0.80	1.90±0.08	533	6.49±0.43	6.42	22 (NNE)	3.87E+22	0.005	30	1869	8.35E+06	1.21E+07	6.58E+06	0.97
2019/9/24	Thu	13.88±1.15	2.14±0.07	533	7.4±0.61	2.96	40 (NE)	4.96E+22	0.01	30	960	7.29E+06	1.22E+07	5.84E+06	0.96
2019/9/28	Sat	11.73±1.70	2.43±0.29	566	6.63±0.96	2.34	28 (NNE)	5.25E+22	-0.001	32	929	5.97E+06	1.18E+07	5.14E+06	0.98
2019/9/29	Sun (work)	10.86±0.98	2.11±0.13	533	5.79±0.52	2.54	88 E	6.87E+22	-0.002	33	1071	5.95E+06	1.12E+07	5.92E+06	0.92
2019/10/1	Tue (holiday)	11.30±1.93	1.57±0.12	533	6.02±1.03	3.29	23 (NNE)	4.32E+22	0	34	862	8.23E+06	1.03E+07	7.96E+06	0.98
2019/10/3	Thu (holiday)	10.30±0.81	1.38±0.15	533	5.48±0.43	1.52	175 (S)	6.11E+22	-0.005	32	1203	8.86E+06	1.03E+07	9.06E+06	0.96
2019/10/18	Fri	11.20±1.35	1.24±0.06	550	6.16±0.74	2.94	325 (NW)	4.27E+22	-0.002	27	1343	8.61E+06	6.99E+06	1.01E+07	0.96

2019/11/3	Sun	10.40±0.62	2.00±0.08	604	6.29±0.37	6.25	359 (N)	5.43E+22	0	26	1231	7.44E+06	6.10E+06	6.25E+06	0.97
2019/11/8	Fri	10.09±1.27	2.82±0.62	559	5.64±0.71	1.2	53 (NE)	2.74E+22	0	24	1539	5.52E+06	5.46E+06	4.43E+06	0.87
2019/11/10	Sun	12.20±1.23	2.38±0.16	604	7.37±0.74	6.07	320 (NW)	5.10E+22	-0.001	25	1270	3.59E+06	6.49E+06	5.25E+06	0.97
2020/1/30	Thu (lockdown & holiday)	3.65±0.36	5.91±026	716	2.61±0.26	2.16	343 (NNW)	4.80E+22	-0.02	15	1066	9.77E+05	1.22E+06	2.12E+06	0.96
2020/1/31	Fri (lockdown &	3.56±0.43	5.44±0.15	716	2.55±0.31	2.92	155 (SSE)	5.13E+22	-0.01	14	794	1.91E+06	1.81E+06	2.30E+06	0.85

	holiday)														
2020/2/5	Wed (lockdown)	2.55±0.31	5.00±0.17	674	1.72±0.21	4.93	105 (ESE)	3.67E+22	0	15	870	3.13E+06	3.14E+06	2.50E+06	0.85
2020/2/9	Sun (lockdown)	2.56±0.33	5.14±0.18	729	1.86±0.24	1.44	272 (W)	4.05E+22	-0.005	15	851	3.10E+06	3.30E+06	2.43E+06	0.9
2020/2/16	Sun (lockdown)	4.20±0.52	3.91±0.35	729	3.06±0.38	5.97	336 (NNW)	1.64E+22	-0.01	7	1365	3.34E+06	3.36E+06	3.20E+06	0.96
2020/2/17	Mon (lockdown)	3.91±0.46	4.05±0.25	674	2.64±0.31	4.56	342 (NNW)	3.32E+22	-0.002	13	1358	3.67E+06	3.45E+06	3.09E+06	0.95
2020/2/20	Thu (lockdown)	3.70±0.45	4.02±0.22	674	2.49±0.3	4.52	124 (SE)	3.48E+22	-0.015	17	956	3.72E+06	4.64E+06	3.11E+06	0.9

2020/3/7	Sat (lockdown)	4.39±0.63	5.24±0.27	663	2.91±0.42	2.39	72 (ENE)	2.94E+22	-0.02	19	660	2.63E+06	4.73E+06	2.39E+06	0.97
2020/3/10	Tue (lockdown)	4.05±0.56	4.13±0.14	625	2.53±0.35	4.94	336 (NNW)	3.00E+22	-0.02	18	1173	2.33E+06	6.69E+06	3.03E+06	0.98
2020/3/17	Tue (lockdown)	4.18±0.76	4.28±0.12	625	2.61±0.47	3.39	273 (W)	2.43E+22	0	21	1356	3.49E+06	7.41E+06	2.92E+06	0.94
2020/3/18	Wed (lockdown)	4.81±0.35	2.63±0.06	625	3±0.22	5.2	225 (SW)	3.43E+22	-0.01	23	1046	4.37E+06	8.11E+06	4.75E+06	0.92
2020/3/19	Thu (lockdown)	4.08±0.49	4.87±0.16	625	2.55±0.31	3.2	36 (NE)	3.63E+22	-0.015	23	1057	3.60E+06	8.66E+06	2.57E+06	0.96
2020/4/9	Thu	5.80±0.63	2.63±0.11	635	3.68±0.4	3.4	179 (S)	5.06E+22	-0.01	27	1465	4.51E+06	9.69E+06	4.75E+06	0.95

2020/4/12	Sun	5.94±0.24	2.43±0.05	674	4±0.16	7.43	311 (NW)	4.59E+22	0	21	1948	5.60E+06	1.03E+07	5.14E+06	0.97
2020/4/13	Mon	6.99±0.78	3.99±0.22	635	4.44±0.5	1.67	272 (W)	5.43E+22	-0.01	22	1719	4.93E+06	9.41E+06	3.13E+06	0.96
2020/4/24	Fri	7.06±0.77	2.28±0.08	635	4.48±0.49	5.39	264 (W)	2.16E+22	0	22	2427	6.58E+06	1.16E+07	5.48E+06	0.92
2020/4/26	Sun (work)	6.68±0.42	1.88±0.18	635	4.24±0.27	5.49	242 (WSW)	3.89E+22	0.001	27	1282	6.45E+06	1.36E+07	6.65E+06	0.89
2020/5/2	Sat (holiday)	7.14±0.97	1.34±0.13	628	4.48±0.61	6.49	238 (WSW)	4.73E+22	-0.01	26	944	8.02E+06	1.75E+07	9.33E+06	0.91
2020/5/3	Sun (holiday)	7.12±0.87	1.47±0.03	640	4.55±0.56	4.35	198 (SSW)	4.10E+22	-0.005	27	1312	7.80E+06	1.85E+07	8.50E+06	0.97
2020/5/10	Sun	7.72±0.91	2.08±0.11	640	4.94±0.58	3.42	324 (NW)	1.44E+22	0.002	27	1370	7.51E+06	1.48E+07	6.01E+06	0.97

2020/5/12	Tue	7.22±0.59	2.08±0.09	592	4.27±0.35	4.1	297 (WNW)	1.56E+2 2	-0.005	30	1693	5.93E+06	1.41E+07	6.01E+06	0.89
2020/5/18	Mon	7.23±1.26	1.89±0.24	592	4.28±0.75	6.91	8 (N)	4.26E+2 2	-0.005	36	1546	7.55E+06	1.61E+07	6.61E+06	0.96
2020/5/23	Sat	7.77±0.39	1.54±0.10	628	4.88±0.24	3.51	197 (SSW)	4.01E+2 2	-0.01	35	1521	8.36E+06	1.78E+07	8.12E+06	0.96
2020/6/3	Wed	8.56±1.02	1.74±0.16	530	4.54±0.54	2.29	107 (ESE)	3.67E+2 2	0	31	969	9.22E+06	1.16E+07	7.18E+06	0.96
2020/6/4	Thu	7.28±0.88	1.89±0.22	530	3.86±0.47	4.54	215 (SW)	2.05E+2 2	-0.01	33	1350	9.95E+06	1.50E+07	6.61E+06	0.95
2020/7/23	Thu	8.45±0.25	0.93±0.04	518	4.38±0.13	4.99	240 (WSW)	2.49E+2 2	-0.005	34	1040	1.23E+07	1.82E+07	1.34E+07	0.87
2020/8/1	Sat	9.73±1.15	1.21±0.12	619	6.02±0.71	4.34	205 (SSW)	3.62E+2 2	-0.02	34	977	1.02E+07	2.06E+07	1.03E+07	0.93
2020/8/3	Mon	8.97±1.05	0.93±0.12	583	5.23±0.61	4.4	201 (SSW)	2.96E+2 2	-0.02	37	1104	1.15E+07	2.14E+07	1.34E+07	0.94

2020/8/14	Fri	8.48±0.84	0.86±0.06	583	4.94±0.49	8.38	213 (SSW)	2.52E+22	-0.02	36	961	9.74E+06	2.03E+07	1.45E+07	0.93
2020/8/18	Tue	8.49±0.74	1.54±0.19	583	4.95±0.43	2.97	191 (S)	3.55E+22	-0.005	35	1151	7.17E+06	2.04E+07	8.12E+06	0.95
2020/8/23	Sun	7.52±0.99	1.48±0.05	630	4.74±0.62	3.86	193 (SSW)	3.01E+22	-0.02	32	941	5.62E+06	1.69E+07	8.45E+06	0.93
2020/8/24	Mon	7.84±0.66	1.44±0.18	583	4.57±0.38	6.87	241 (WSW)	2.75E+22	-0.02	34	1020	7.68E+06	1.88E+07	8.68E+06	0.91
2020/8/26	Wed	8.61±1.13	1.44±0.13	583	5.02±0.66	5.19	340 (NNW)	3.08E+22	0	31	1039	1.08E+07	1.55E+07	8.68E+06	0.96
2020/8/27	Thu	8.55±0.66	1.56±0.05	583	4.98±0.38	2.52	42 (NE)	3.48E+22	0	33	841	9.59E+06	1.45E+07	8.01E+06	0.95
2020/8/28	Fri	9.10±0.84	1.75±0.23	583	5.3±0.49	2.37	46 (NE)	3.81E+22	0	33	1089	8.54E+06	1.71E+07	7.14E+06	0.93
2020/8/29	Sat	8.85±0.72	1.67±0.24	619	5.47±0.45	4.39	36 (NE)	3.13E+22	0	33	1028	7.39E+06	1.72E+07	7.49E+06	0.94

References

Bovensmann, H., Buchwitz, M., Burrows, J. P., Reuter, M., Krings, T., Gerilowski, K., Schneising, O., Heymann, J., Tretner, A., and Erzinger, J.: A remote sensing technique for global monitoring of power plant CO_2 emissions from space and related applications, Atmos. Meas. Tech., 3, 781-811, 10.5194/amt-3-781-2010, 2010.

Hersbach, H., Bell, B., Berrisford, P., Hirahara, S., Horányi, A., Muñoz - Sabater, J., Nicolas, J., Peubey, C., Radu, R., Schepers, D., Simmons, A., Soci, C., Abdalla, S., Abellan, X., Balsamo, G., Bechtold, P., Biavati, G., Bidlot, J., Bonavita, M., Chiara, G., Dahlgren, P., Dee, D., Diamantakis, M., Dragani, R., Flemming, J., Forbes, R., Fuentes, M., Geer, A., Haimberger, L., Healy, S., Hogan, R. J., Hólm, E., Janisková, M., Keeley, S., Laloyaux, P., Lopez, P., Lupu, C., Radnoti, G., Rosnay, P., Rozum, I., Vamborg, F., Villaume, S., and Thépaut, J. N.: The ERA5 global reanalysis, Q J R Meteorol Soc., 146, 1999-2049, 10.1002/qj.3803, 2020.

Liu, F., Beirle, S., Zhang, Q., Dörner, S., He, K., and Wagner, T.: NO_x lifetimes and emissions of cities and power plants in polluted background estimated by satellite observations, Atmos. Chem. Phys., 16, 5283-5298, 10.5194/acp-16-5283-2016, 2016.

Lorente, A., Boersma, K. F., Eskes, H. J., Veefkind, J. P., van Geffen, J., de Zeeuw, M. B., Denier van der Gon, H. A. C., Beirle, S., and Krol, M. C.: Quantification of nitrogen oxides emissions from build-up of pollution over Paris with TROPOMI, Sci. Rep., 9, 20033, 10.1038/s41598-019-56428-5, 2019.

Masters, G. M. and Ela, W. P.: Introduction to environmental engineering and science, Pearson, 3rd edition pp. 457, 2007.

Zheng, B., Chevallier, F., Ciais, P., Broquet, G., Wang, Y., Lian, J., and Zhao, Y.: Observing carbon dioxide emissions over China's cities and industrial areas with the Orbiting Carbon Observatory-2, Atmos. Chem. Phys., 20, 8501-8510, 10.5194/acp-20-8501-2020, 2020.